Computer-Aided Design of a Brushless DC Motor with Exterior-Rotor Configuration

Yi-Chang Wu and Bo-Wei Lin

National Yunlin University of Science & Technology, wuyc@yuntech.edu.tw

ABSTRACT

The aim of this paper is to evaluate the magnetic field and motor performance of an exterior-rotor brushless DC (BLDC) motor based on two approaches, i.e., the magnetic circuit method and the finite-element analysis (FEA). An equivalent magnetic circuit model is applied to analytically estimate the magnetic field of a BLDC motor, while the validity is verified by the two-dimensional FEA. Due to the restriction of the simplified mathematical model, the FEA is further employed to be an assistant tool for the detailed design of the pole shoe of this BLDC motor. Four design cases with different pole shoe dimensions are proposed, and the one that possesses the largest electromagnetic torque as well as the smallest cogging torque and torque ripple is further prototyped for electric bicycle applications.

Keywords: computer-aided design, finite-element analysis, brushless DC motor.
DOI: 10.3722/cadaps.2012.457-469

1 INTRODUCTION

Brushless DC (BLDC) motors have been one of the focuses of research and development of electric motors due to the rapid development of permanent magnets with high energy product. The BLDC motor is a kind of brushless permanent-magnet motor with the trapezoidal back electromotive force (back-EMF) waveform and rectangular excitation current [4]. It has attracted extensive interest due to the characteristics of high efficiency, light weight, low cost of maintenance, easy speed control, and low noise and vibration. Thus, BLDC motors are widely employed for the purpose of constant speed and high-precision position control. For motor designers, the analysis of the magnetic field is a major concern to predict the motor performance before actually fabricating the prototype. Generally, there are two major approaches for the magnetic field approximations of electric motors, i.e., the analytical technique and the numerical method. The analytical technique is ideally based on the assumptions of material linearity and no saturation occurred in the motor for solving the magnetic field. The equivalent magnetic circuit method with lumped circuit parameters is one of the analytical techniques

to predict the open-circuit magnetostatic field by simplifying the motor topology. According to the closed flux loops, an equivalent magnetic circuit model can be set up, which provides engineers sufficient insight into the effects of design parameters on the magnetic characteristics, especially in the preliminary design stage. Qu and Lipo [5] analyzed and modeled the magnetic field of the surface-mounted permanent-magnet motor with a radial-flux topology. The air-gap leakage flux, which is an essential quantity for the accurate prediction of the machine torque, is analytically expressed in terms of magnetic material properties and motor dimensions. Yang et al. [9],[10] presented the magnetic circuit model of a disk-type axial-flux BLDC motor for electric vehicles, in which electromagnetic properties, including the flux density of the air gap, co-energy, and output torque, are derived with sensitivity analyses. In addition to the analytical techniques, numerical methods for magnetic field computation [2],[3],[7],[8], such as the finite-difference method, the boundary-element method, and the finite-element method, also provide accurate means of determining the flux density distribution. These methods are commonly called the finite-element analysis (FEA). The FEA is a powerful and reliable tool to deal with the design of electric motors before fabricating actual prototypes. The main features of the FEA are the capabilities of solving magnetic fields with nonlinear magnetic material properties, coupled physical fields, and complex motor geometries. It is preferred to be an assistant tool for confirming or improving the results of analytical works.

The purpose of this paper is to evaluate the magnetic field and motor performance of an exterior-rotor BLDC motor used for electric bicycles. The equivalent magnetic circuit model [5] is employed to analytically analyze the magnetic field of a BLDC motor. The two-dimensional FEA is then applied to verify the validity of the analytical results. Due to the inherent restriction of the simplified motor topology of the equivalent magnetic circuit model, the FEA is further used in the detail design stage to assist in evaluating proper dimensions of the pole shoe of this motor. Among four design cases, the one with better motor performance is prototyped for further testing.

2 AN EXTERIOR-ROTOR BLDC MOTOR

The BLDC motor is essentially configured as alternate magnet poles rotating past stationary conductors that carry the current. Fig. 1 shows a cross-sectional view of the proposed 3-phase, 20-pole/18-slot exterior-rotor BLDC motor used in the power system of an electric bicycle. Permanent magnets are affixed to the inner surface of the rotor yoke, which prevents the magnets from flying apart especially in high-speed applications. Since the cross-section of the exterior-rotor BLDC motor is identical with the permanent-magnet DC commutator motor, DC armature winding machines can easily be adopted to wind the stator. The main features of such an exterior-rotor design are simple to wind and easy to manufacture, which results in low product cost. In addition, the relative large rotor diameter increases the moment inertia, which in turn helps to maintain constant rotational speed. This kind of motor configuration is also suitable for data storage hard-disk drives, cooling fans, blowers, and directly driven wheel motor for electric scooters and vehicles, **é** etc.

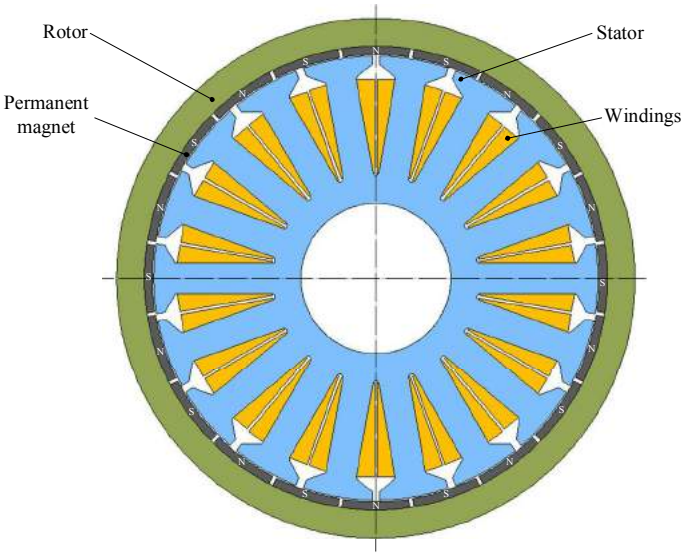

Fig. 1: Cross-section of a 3-phase, 20-pole/18-slot BLDC motor with exterior rotor configuration.

3 ANALYSIS OF MAGNETIC FIELD AND MOTOR PERFORMANCE

The equivalent magnetic circuit approach with lumped parameters is an analytical technique to predict the open-circuit magnetostatic field of electric motors. Fig. 2 shows the linear translational topology of the BLDC motor depicted in Fig. 1 and the related flux paths. The main flux or air-gap flux Φ_g crosses the air gap and links the coils of the phase windings on the stator. The magnet flux Φ_m is the flux actually passing through the magnet, which is equal to the summation of the air-gap flux and the leakage flux. As depicted in Fig. 2, the leakage flux generally consists of two parts, i.e., the magnet-to-rotor leakage flux Φ_{mr} and the magnet-to-magnet leakage flux Φ_{mm}. The leakage flux is an essential quantity for accurately predicting average flux densities within the air gap and the magnet as well as the electromagnetic torque of the electric motor. To simplify the analysis, it is assumed that there is no magnetic saturation occurring in the steel region and the magnetic field intensity produced by the armature current in the stator windings is negligible. Besides, the stator and rotor back irons are with infinite permeability. Analogous to the Ohm's law in electricity, the equivalent magnetic circuit of this BLDC motor is shown in Fig. 3(a) [5]. It is composed of one-half of two magnets and the associated rotor and stator back iron halves for providing flux return paths. In the figure, $\Phi_r/2$ is the flux source of one-half of a magnet, $\Phi_g/2$ is the air gap flux flowing through one-half of the air gap cross-sectional area, and $\Phi_m/2$ is the flux leaving the one-half magnet, respectively. R_r and R_s are the reluctances of the rotor and stator back irons, respectively. $2R_g$ is the reluctance of the one-half of the air gap. $2R_{mo}$ is the reluctance of one-half of a magnet. R_{mm} and R_{mr} are the reluctances modeling the flux leakage from magnet to magnet as well as magnet to rotor, respectively. Due to the assumption of infinite permeability for the rotor and stator back irons, the values of R_r and R_s can be ignored. Fig. 3(b) shows the simplification of the magnetic circuit, where R_m can be expressed as:

$$R_m = R_{mo}/(1+2\eta+4\lambda) \tag{3.1}$$

where

$$\eta = R_{mo}/R_{mr} \tag{3.2}$$

and

$$\lambda = R_{mo} / R_{mm} \tag{3.3}$$

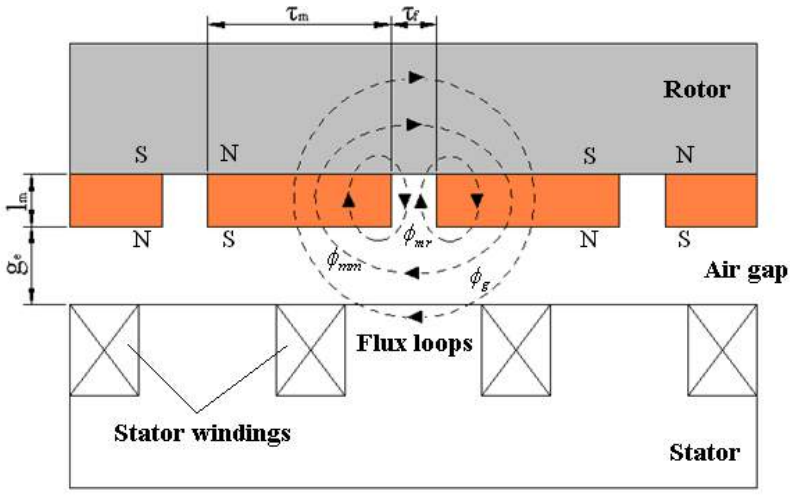

Fig. 2: Linear translational topology of the BLDC motor shown in Fig. 1.

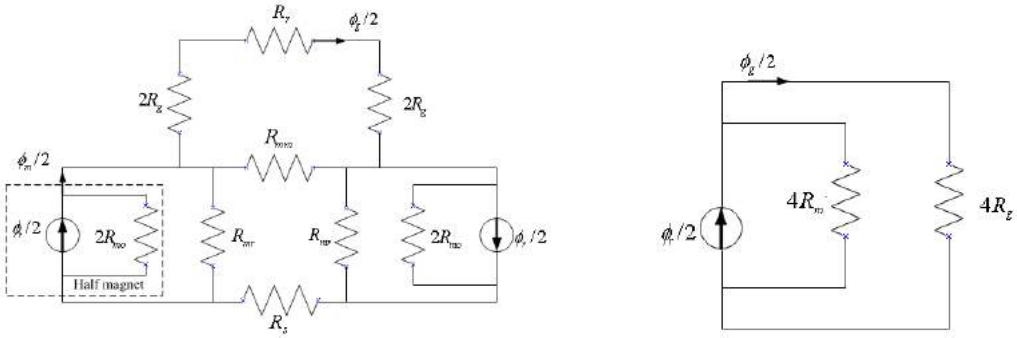

(a) (b)

Fig. 3: Equivalent magnetic circuit and the corresponding reduced form [5].

Simultaneously, the air gap flux Φ_g is derived as:

$$\phi_g = \frac{R_m \phi_r}{R_m + R_g} = \frac{R_{mo}}{R_{mo} + R_g(1 + 2\eta + 4\lambda)} \phi_r \tag{3.4}$$

The flux leaving the magnet is further obtained as:

$$\phi_m = \frac{R_{mo} + R_g(2\eta + 4\lambda)}{R_{mo} + R_g(1 + 2\eta + 4\lambda)} \phi_r \tag{3.5}$$

In addition, the flux source of the magnet Φ_r is written as:

$$\phi_r = A_m B_r \tag{3.6}$$

where A_m and B_r represent the flux passing area and the residual flux density of the magnet, respectively. Based on Eqns. (3.4)-(3.6), the average flux densities within the air gap and the magnet are:

$$B_{g,ave} = \frac{A_m / A_g}{1 + (R_g / R_{mo})(1 + 2\eta + 4\lambda)} B_r \tag{3.7}$$

and

$$B_m = \frac{1 + (R_g / R_{mo})(2\eta + 4\lambda)}{1 + (R_g / R_{mo})(1 + 2\eta + 4\lambda)} B_r \tag{3.8}$$

where A_m/A_g is the ratio of the magnetic flux passing area of the magnet to that of the air gap. Besides, the following expressions are also obtained based on geometric and magnetic relationships.

$$A_m = \tau_m L \tag{3.9}$$

$$A_g = (\tau_m + \tau_f) L \tag{3.10}$$

$$R_{mo} = l_m / (\mu_o \mu_r A_m) \tag{3.11}$$

$$R_g = g_e / [\mu_o (\tau_m + 2g_e) L] \tag{3.12}$$

$$g_e = k_c g \tag{3.13}$$

where L is the stack length of the stator, τ_m is the magnet width, τ_f is the length of two adjacent magnets, l_m is the magnet height, μ_0 is the permeability of free space, μ_r is the relative permeability of the magnet, g and g_e are the air gap length and effective air gap length, respectively, and k_c is the Carter's coefficient [1]. In particular, the fringing effect is taken into consideration by adding the length $2g_e$ to τ_m for the calculation of R_g shown in Eqn. (3.12). The magnet-to-rotor and magnet-to-magnet reluctances, i.e., R_{mr} and R_{mm}, shown in Eqn. (3.2) and Eqn. (3.3) can be further obtained by calculating their permeances using corresponding circular-arc, straight-line permanence models [5]. They can be derived as:

$$R_{mr} = \frac{1}{P_{mr}} = \frac{1}{\frac{\mu_o L}{\pi} \ln[1 + \frac{\pi \min(g_e, \tau_f / 2)}{l_m}]} \tag{3.14}$$

$$R_{mm} = \frac{1}{P_{mm}} = \frac{1}{\frac{\mu_o L}{\pi} \ln(1 + \frac{\pi g_e}{\tau_f})} \tag{3.15}$$

where $\min(g_e, \tau_f / 2)$ is the minimum function. Based on Eqns. (3.9), (3.11), (3.14), and (3.15), Eqns. (3.2) and (3.3) are further rewritten as:

$$\eta = \frac{l_m}{\mu_r \pi \tau_m} \ln(1 + \frac{\pi \min(g_e, \tau_f / 2)}{l_m}) \tag{3.16}$$

$$\lambda = \frac{l_m}{\mu_r \pi \tau_m} \ln(1 + \frac{\pi g_e}{\tau_f}) \tag{3.17}$$

Eventually, the magnetic flux densities within the air gap and the magnet are obtained, by substituting Eqns. (3.9)-(3.13), (3.16), and (3.17) into Eqns. (3.7) and (3.8) with some algebraic manipulation, as follows [5]:

$$B_{g,ave} = \frac{B_r}{1 + \frac{\tau_f}{\tau_m} + \mu_r \frac{g_e}{l_m} \frac{\tau_m + \tau_f}{\tau_m + 2g_e}(1 + 2\eta + 4\lambda)} \tag{3.18}$$

and

$$B_m = \frac{(1 + \frac{2g_e}{\tau_m}) \frac{1}{\mu_r} \frac{l_m}{g_e} + 2\eta + 4\lambda}{(1 + \frac{2g_e}{\tau_m}) \frac{1}{\mu_r} \frac{l_m}{g_e} + 1 + 2\eta + 4\lambda} \tag{3.19}$$

The accurate computation of the air gap flux density, in fact, is essential for the accurate prediction of the motor performance. Once the average flux density within the air gap is given, the average back-EMF constant, K_e, and average electromagnetic torque, T_{ave}, of a BLDC motor can be expressed as follows [1, 6]:

$$k_e = k_w N_{tol} B_{g,ave} R_{ri} L \tag{3.20}$$

$$T_{ave} = m k_l k_w N_{tol} B_{g,ave} R_{ri} L i_{ph} \tag{3.21}$$

where k_w is the winding factor, N_{tol} is the total conductors per phase, R_{ro} is the outside rotor radius, m is the phases of conduction, k_l is the correction factor due to losses, and i_{ph} is the phase current, respectively. The winding factor can be further expressed as:

$$k_w = \frac{\sqrt{(\sum_{i=1}^{N} \sin\theta_i)^2 + (\sum_{i=1}^{N} \cos\theta_i)^2}}{N_{tol}} \tag{3.22}$$

where θ_i is the related electrical angle of the ith conductor of this phase.

In order to meet desired requirements of electric bikes, the output torque of the motor should not less than 13Nm. Based on the above derived formulations, Tab. 1 shows a set of feasible solutions for the values of magnet properties and main dimensions of the proposed BLDC motor, while the related geometric parameters are depicted in Fig. 4(a). The analytical results of magnetic field and motor performance, including g_e, η, λ, $B_{g,ave}$, B_m, k_w, k_e, and T_{ave}, are respectively listed in Tab. 2. In order to make a quantitative comparison with the analytical results, the FEA is applied to assist in numerically calculating the magnetic field and the electromagnetic torque. The ANSOFT/Maxwell 2D field simulator is employed to the field analysis of this motor. Fig. 4(b) demonstrates the finite element meshing of this motor, where the total numbers of triangle mesh elements is 64,814. The winding

layout for this 3-phase, 20-pole/ 18-slot BLDC motor is listed in Fig. 5(a), while the winding configuration is schematically shown in Fig. 5(b). Each phase has six concentrated coils connected in series. Since the number of windings per phase is six and each winding has two groups of conductors, the total conductors per phase becomes N_{tol} =12N_c. The excitation current is operated with square wave as shown in Fig. 6, where two phases conduct simultaneously at each time, i.e., m=2. Fig. 7 presents the waveforms of the three-phase back-EMF constant without multiplying the number of coils. It is apparent that the back-EMF constant is similar to a trapezoidal wave shape. The flux density distributions in the air gap and the electromagnetic torque of this BLDC motor are illustrated in Figs. 8 and 9, respectively.

Magnet properties		
Items	Symbol	Values
Remanence (T)	B_r	0.76
Coercivity (A/m)	H_c	-480000
Relative permeability	μ_r	1.26
Direction of magnetization	--	radial
Magnet thickness (mm)	l_m	3
Magnet arc (degree)	θ_m	17
Motor parameters		
Items	Symbol	Values
Number of phases	N_{ph}	3
Number of magnet poles	N_m	20
Number of magnet slots	N_s	18
Air gap length (mm)	g	0.5
Slot opening width of stator (mm)	w_s	2.8
Outer radius of rotor (mm)	R_{ro}	93.5
Inner radius of rotor (mm)	R_{ri}	80.5
Outer radius of stator (mm)	R_{so}	80
Inner radius of stator (mm)	R_{si}	27
Tooth width of stator (mm)	W_{tb}	11
Shoe depth (mm)	d_1	5
Shoe ramp (degree)	d_2	15
Number of coils per armature tooth (turn)	N_c	36
Stack length (mm)	L	24
Rated phase current (A)	i_{ph}	14.8

Tab. 1: Corresponding values of magnet properties and main dimensions of the BLDC motor.

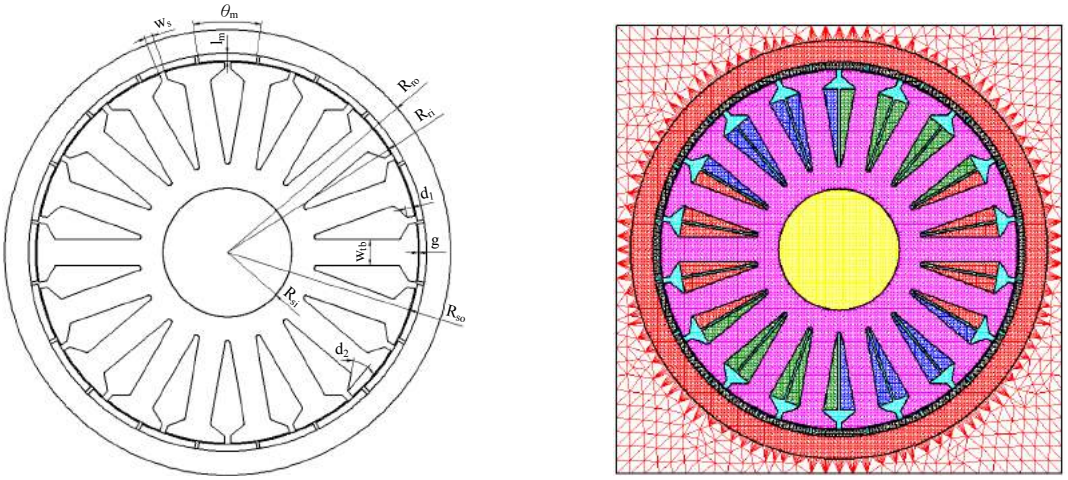

(a) (b)

Fig. 4: Geometric parameters and finite element meshing of the exterior-rotor BLDC motor.

Slot	Phase A	Phase B	Phase C
1	In & In		
2	Out & Out		
3	In		Out
4			In & In
5			Out & Out
6		Out	In
7		In & In	
8		Out & Out	
9	Out	In	
10	In & In		
11	Out & Out		
12	In		Out
13			In & In
14			Out & Out
15		Out	In
16		In & In	
17		Out & Out	
18	Out	In	

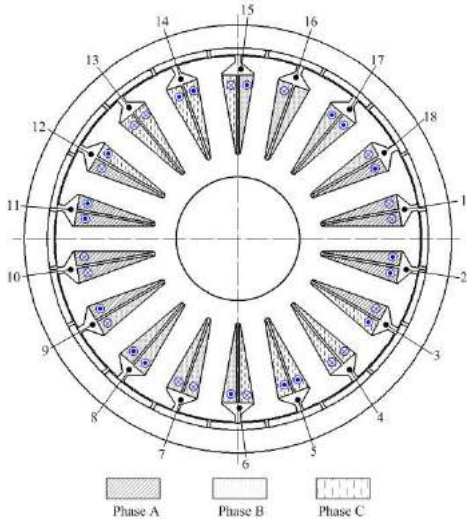

(a) (b)

Fig. 5: Winding layout and winding configuration of the BLDC motor.

Items	Symbol	Values
Magnet width (mm)	τ_m	24.3299
Length of two adjacent magnets (mm)	τ_f	1.4312
Effective air gap length (mm)	g_e	0.5328
Reluctance ratio of a magnet pole to the magnet-to-rotor leakage flux	η	0.0138
Reluctance ratio of a magnet pole to the magnet-to-magnet leakage flux	λ	0.0241
Average magnetic flux densities within the air gap (T)	$B_{g,ave}$	0.5784

Average magnetic flux densities within the magnet (T)	B_m	0.6287
Total conductors per phase	N_{tol}	432
Winding factor	k_w	0.945
Average back-EMF constant (V/rad/s)	k_e	0.4562
Average electromagnetic torque (Nm)	T_{ave}	13.5034

Tab. 2: Analysis of magnetic field and motor performance of the BLDC motor shown in Fig. 1.

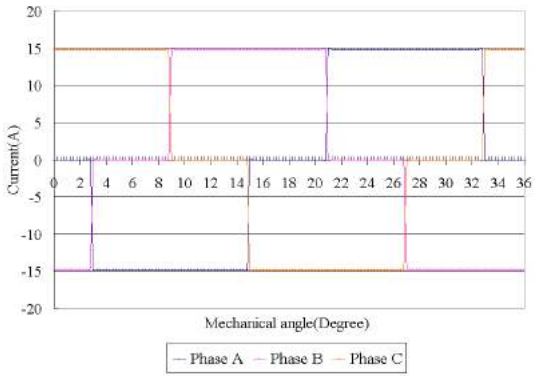

Fig. 6: Three-phase excitation current waveforms. waveforms.

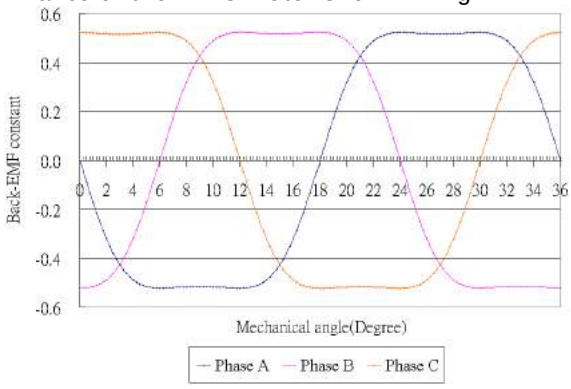

Fig. 7: Three-phase back-EMF constant

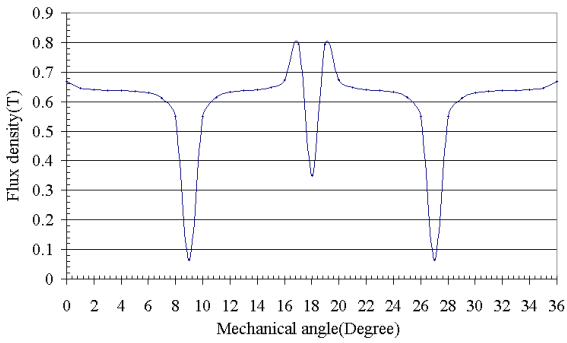

Fig. 8: Air gap flux density waveform.

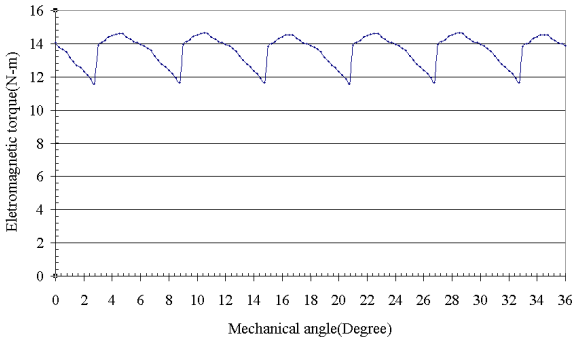

Fig. 9: Electromagnetic torque.

By comparing the FEA results with the analytical computations, Tab. 3 gives the errors between these two methods. It shows that the results are in good agreement with a maximum error of about 3%. Therefore, the equivalent magnetic circuit method is an acceptable technique in predicting the magnetic field and performance of BLDC motors. It also provides enough insight and clear relationships to the field distribution, magnetic material properties, and machine dimensions. Although the equivalent magnetic circuit method is a suitable and fast tool for the preliminary design of BLDC motors, it does not provide sufficient information to deal with the effects of pole shoes on the magnetic field and motor performance due to the simplified motor topology shown in Fig. 2. Due to this reason, the FEA is preferred to confirm or improve the results of analytical design works particularly in the detail design stage.

Items	Symbol	Analytical results	FEA results	Error (%)
Average magnetic flux densities within the air gap (T)	$B_{g,ave}$	0.5784	0.5957	-2.9910
Average magnetic flux densities within the magnet (T)	B_m	0.6287	0.6263	0.3817
Average back-EMF constant (V/rad/s)	k_e	0.4562	0.4628	-1.4467
Average electromagnetic torque (Nm)	T_{ave}	13.5034	13.5917	-0.6539

*Error= (Analytical result- FEA result)/ Analytical result*100%

Tab. 3: Comparison of analytical results and FEA results.

4 COMPUTER-AIDED DESIGN OF THE POLE SHOE

In this section, four design cases with different values of the shoe depth and the shoe ramp, i.e., parameters d_1 and d_2 shown in Fig. 4(a) are proposed in Tab. 4 and Fig. 10. The FEA is employed to be an assistant tool for the computer-aided design of the pole shoe of this BLDC motor. Fig.11 presents the distributions of cogging torques for these four cases. The cogging torque of the permanent-magnet motor arises from the interaction of permanent magnets and the stator slotted structure without the applied driving current. Since it is an oscillatory torque that always induces vibration, acoustic noise, and possible resonance especially at high load and low speed, the reduction of the cogging torque is really an important task for motor designers. From the simulation results, Case I possesses smaller cogging torque than others. Fig. 12 and Tab. 4 respectively show the electromagnetic torque and torque ripple of each design case. As can be seen, Case I has the largest electromagnetic torque and the smallest torque ripple among them. Hence, Case I is preferable to be prototyped. Fig. 13 shows the explored view of the design case I by commercial computer-aided design package SolidWorks, while Fig.14 presents the prototype of this motor for electric bicycle applications.

Case	Parameters of the pole shoe	Average electromagnetic torque (Nm)	Torque ripple (%)
I	$d_1 = 3mm, d_2 = 30°$	13.87	20.67
II	$d_1 = 5mm, d_2 = 0°$	13.63	21.55
III	$d_1 = 5mm, d_2 = 15°$	13.59	22.27
IV	$d_1 = 6mm, d_2 = 0°$	13.45	22.81

Tab. 4: Average electromagnetic torque and torque ripple of proposed four design cases.

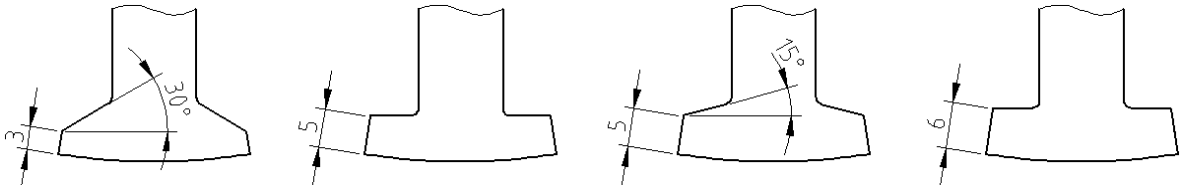

Case I Case II Case III Case IV

Fig. 10: Four design cases with different values of the shoe depth and the shoe ramp.

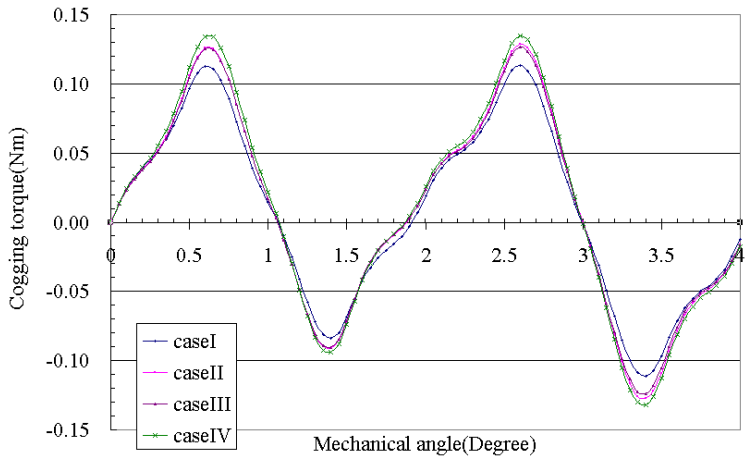

Fig. 11: Cogging torque distributions of the proposed four design cases.

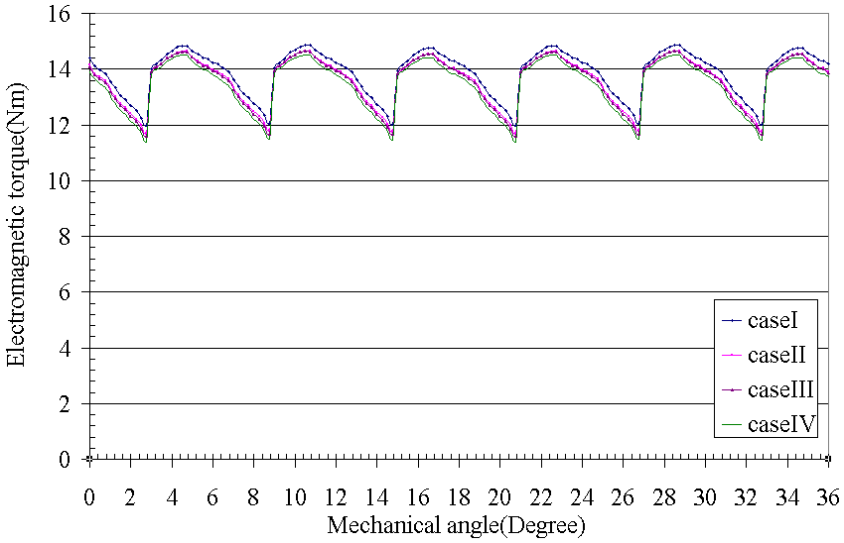

Fig. 12: Electromagnetic torques of the proposed four design cases.

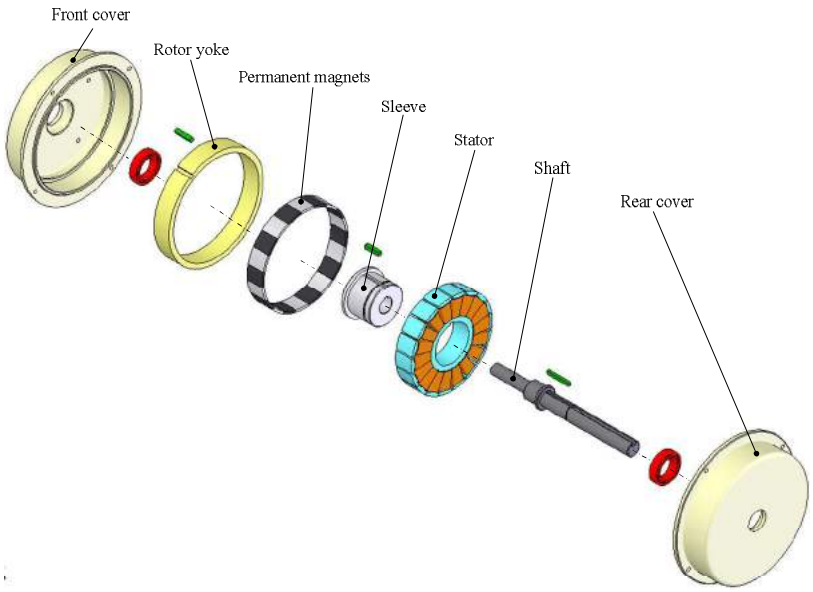

Fig. 13: Explored view of the design case I for the proposed BLDC motor.

Fig. 14: The prototype of Case I for the proposed BLDC motor.

5 CONCLUSION

In this paper, the magnetic field and motor performance of an exterior-rotor BLDC motor used for electric bicycles has been analyzed by both utilizing the equivalent magnetic circuit method and the finite-element method. Although the equivalent magnetic circuit method is a suitable and fast tool for the preliminary design and analysis of BLDC motors, it does not provide sufficient information to deal with the effects of pole shoes on the magnetic field and motor performance due to the simplified motor topology. The FEA is further employed to overcome this drawback particularly in the detail design stage. Among four design cases, Case I possesses a higher electromagnetic torque and lower cogging torque and torque ripple. The solid model and corresponding engineering drawings of Case I are constructed by commercial computer-aided design software. Besides, it is also prototyped for further performance testing. The results of this study are helpful in the development of BLDC motors with interior-rotor or exterior-rotor configurations.

ACKNOWLEDGEMENTS

The authors are grateful to the National Science Council (Taiwan, R.O.C) for supporting this research under grants NSC 99-2221-E-224-011 and NSC 100-2221-E-224-023.

REFERENCES

[1] Hanselman, D.: Brushless Permanent-Magnet Motor Design 2nd Edition, The Writers' Collective, Rhode Island, 2003.

[2] Hsu, Y. S.; Tsai, M. C.; Hsieh, M. F.: Novel Stator Design of Fan Motors Using Soft Magnetic Composites, Journal of Applied Physics, 103(7), 2008, Paper No. 07F109. DOI: 10.1063/1.2831498

[3] Lacombe, G.; Foggia, A.; Marechal, Y.; Brunotte, X.; Wendling P.: From General Finite-Element Simulation Software to Engineering-Focused Software: Example for Brushless Permanent Magnet Motors Design, IEEE Transactions on Magnetics, 43(4), 2007, 1657-1660. DOI: 10.1109/TMAG.2007.892495

[4] Miller, T. J. E.; Hendershot, Jr., J. R.: Design of Brushless Permanent Magnet Motors, Clarendon Press, Oxford, 1994.

[5] Qu, R.; Lipo, T. A.: Analysis and Modeling of Air-Gap and Zigzag Leakage Fluxes in a Surface-Mounted Permanent-Magnet Machine, IEEE Transactions on Industry Applications, 40(1), 2004, 121-127. DOI:10.1109/TIA.2003.821790

[6] Tsai, M. C.; Weng, M. H.; Hsieh, M. F.: Computer-Aided Design and Analysis of New Fan Motors, IEEE Transactions on Magnetics, 38(5), 2002, 3467-3474. DOI:10.1109/TMAG.2002.802713

[7] Wrobel, R.; Mellor, P. H.: Design Considerations of a Direct Drive Brushless Machine with Concentrated Windings, IEEE Transactions on Energy Conversion, 23(1), 2008, 1-8. DOI:10.1109/TEC.2007.905073

[8] Yan, G. J.; Hsu, L. Y.; Wang, J. H.; Tsai, M. C.; Wu, X. Y.: Axial-Flux Permanent Magnet Brushless Motor for Slim Vortex Pumps, IEEE Transactions on Magnetics, 45(10), 2009, 4732-4735.

[9] Yang, Y. P.; Luh, Y. P.; Lee, C. M.: A Novel Design of Optimal Phase Current Waveform for an Electric Vehicle Wheel Motor, Electric Power Components and Systems, 30, 2002, 705-721. DOI: 10.1080/15325000290085136

[10] Yang, Y. P.; Luh, Y. P.; Cheung, C. H.: Design and Control of Axial-Flux Brushless DC Wheel Motors for Electric Vehicles- Part I: Multiobjective Optimal Design and Analysis, IEEE Transactions on Magnetics, 40(4), 2004, 1873-1882. DOI:10.1109/TMAG.2004.828164